Verma *et al.*
*Protection and Control of Modern Power Systems* (2023) 8:32
https://doi.org/10.1186/s41601-023-00309-7

Protection and Control of Modern Power Systems

ORIGINAL RESEARCH

Open Access

# Battery energy storage-based system damping controller for alleviating sub-synchronous oscillations in a DFIG-based wind power plant

Neevatika Verma[1], Narendra Kumar[1] and Rajeev Kumar[2,3*]

**Abstract**

This paper presents the issue of the Sub-synchronous resonance (SSR) phenomenon in a series compensated DFIG-based wind power plant and its alleviation using a Battery Energy Storage-based Damping Controller ($BESSDC_L$). A supplementary damping signal is developed considering the angular speed deviation and is incorporated into the BESS control system. Wide-area Measurement System data is used to determine the angular speed deviation. A linearized system model is developed to perform eigenvalue analysis, and to detect and examine unstable SSR modes. The variation of wind speed and three-phase fault are also taken into consideration to validate the robustness of the controller. To further verify the efficacy of the proposed damping controller, time-domain simulations are performed using MATLAB/Simulink. The application of the proposed $BESSDC_L$ stabilizes all the unstable system modes effectively at wind speeds of 7 m/s, 9 m/s, and 11 m/s, and at 40%, 50%, and 60% series compensation levels, as well three-phase fault conditions.

**Keywords** Battery energy storage system, Damping controller, Doubly-fed induction generator (DFIG), Series compensation, Sub-synchronous resonance (SSR)

## 1 Introduction

The world is now focusing on renewable energy sources. One of the best-paying and most accessible sources of energy is wind. The areas where wind energy is abundant are generally very remote to power-demand areas. Thus, new wind energy power plants can be integrated into the existing national grid through dedicated or existing transmission lines by increasing the power transfer capability using fixed series compensation (FSC) or FACT devices [1]. Installing FSC in a long transmission line is an inexpensive and efficient way to improve the capability of power transfer of an existing transmission line [2]. However, the problem that may arise because of FSC in a long transmission line is Sub-synchronous resonance (SSR), which can lead to shaft failure and power system instability [3, 4]. Various historical events have already been reported in which the undamped SSR outcomes caused the complete failure of generator rotor shafts. The first two incidents happened in the Mohave power plant, in Nevada, USA, in 1970 and 1971, [5], and the first event occurred in the wind plant in October 2009 at Zorillo Gulf Wind Farm, Texas [6]. Following these incidents, the research community has focused on finding ways to deal with the SSR problem.

*Correspondence:
Rajeev Kumar
rajeev.rakshit@gmail.com
[1] Department of Electrical Engineering, Delhi Technological University, New Delhi, India
[2] Electrical Engineering Department, Jamia Millia Islamia, New Delhi, India
[3] Electrical and Electronics Engineering Department, KIET Group of Institutions, Ghaziabad, India

© The Author(s) 2023. **Open Access** This article is licensed under a Creative Commons Attribution 4.0 International License, which permits use, sharing, adaptation, distribution and reproduction in any medium or format, as long as you give appropriate credit to the original author(s) and the source, provide a link to the Creative Commons licence, and indicate if changes were made. The images or other third party material in this article are included in the article's Creative Commons licence, unless indicated otherwise in a credit line to the material. If material is not included in the article's Creative Commons licence and your intended use is not permitted by statutory regulation or exceeds the permitted use, you will need to obtain permission directly from the copyright holder. To view a copy of this licence, visit http://creativecommons.org/licenses/by/4.0/.

The evolution of damping the SSR starts with designing a power system stabilizer that can provide a proper phase shift between the exciter circuit and the mechanical system [7]. The damping technology obtained by designing the controller was not very effective as the controller response was sluggish. With the advance of power electronic-based devices and the use of FACTS devices, new controllers have been designed to have a faster response [8, 9, 10, 1211 and ]. In this context, Damping Controllers (DCL) were developed to be used with the UPFC's main controller [13], while a Band-Pass Filter- (BPF) based DCL was developed for SSSC devices to eliminate the SSR in a system having a non-identical parallel interconnected generator [11]. Sub-synchronous oscillation was minimized over a broad range for MMC-STATCOM using an additional wide-band damping control approach, in which a notch filter was used to filter fundamental frequencies and provide a damping control signal for Sub-synchronous frequencies [14]. To optimize the parameters of the fundamental controller employed in the STATCOM control system, a BFOA (Bacterial Foraging Optimization Algorithm)-based optimal controller was proposed [15]. However, the usage of FACTS devices for damping the oscillations is practically limited since operational maintenance and installation of these devices may not be economically efficient [16]. An adaptive supplementary damping controller-based Phase-locked Loop (PLL), which is simple in structure with simple parameter control and flexibility in adapting to different operating modes, was used in wind power plants to address the problems of cost control and difficult parameter control [17]. Reference [18] suggested Variable-gain Super-twisting Sliding Mode Control (VGSTSMC) of DFIG-based WPP to reduce Sub-synchronous control interactions and maintain power system stability. An energy-shaping L2-gain Controller (ESLGC) for direct-driven PMSG converters was employed in [19], in which the ESLGC increases system robustness against disturbances while simultaneously ensuring global asymptotical stability. To address the SSR issue in DFIG-based WPP, a nonlinear Sliding Mode Control (SMC) was implemented in the rotor side converter (RSC) [20]. The use of the Whale Optimization Algorithm (WOA) for controller tuning was studied in [21], to accomplish one degree of freedom, namely pitch angle and external resistance connected to the rotor of the generator, in order to reduce SSR.

In recent years, the increasing use of Battery Energy Storage Systems (BESS) in power systems has led researchers to focus on the application of BESS to provide balance and steady operation of devices in dynamic power generation and consumption. Using BESS for SSR damping offers many advantages, including quick response time, flexibility, cost-effectiveness, scalability, and redundancy. These benefits make BESS an effective solution to mitigate SSR in power systems. Here are some benefits for using BESS for SSR damping purposes:

1. *Quick response time* BESS has a very fast response time compared to traditional mitigating techniques. BESS can respond within milliseconds to a change in system conditions, providing an effective solution to dampen the oscillations caused by SSR.
2. *Flexibility* BESS is a flexible solution for SSR damping purposes. The amount and phase angle of reactive power injected or absorbed by BESS can be easily controlled using power electronics converters. This flexibility allows BESS to provide precise and efficient SSR damping support.
3. *Scalability* BESS can be scaled up or down as needed, making them a scalable solution for power systems of different sizes.
4. *Cost-effective* The cost of BESS has decreased over the years, making them a more cost-effective solution for SSR damping than traditional solutions like synchronous condensers or FACTS. BESS can be more cost-effective in terms of installation, operation, and maintenance costs.
5. *Redundancy* In the event of a failure of a BESS unit, other BESS units can take over, ensuring system stability and reliability.
6. *Reducing transmission losses* By injecting or absorbing reactive power, a BESS can help reduce transmission losses and improve the overall efficiency of the power system.

However, the extent of this technology is yet to be explored. Previously, SSR was mitigated using Superconducting Magnetic Energy Storage (SMES) by managing the active and reactive power of the system lines [22]. Nonetheless, BESS not only provides the optimal storage of renewable energy but is also responsible for the smooth variation of PV, load shedding, and supply–demand power response [23]. A conventional BESS comprises a step-up coupling transformer, a passive inductive filter, a DC/AC power converter, and a battery bank. Because of the low cost of BESS and its constraint-free installation, it has become increasingly popular. However, there is still limited research on controller design using BESS technology to dampen SSR. Solutions were proposed for BESS to attenuate inter-area oscillation [24], whereas an optimization approach was suggested for appropriately positioning the BESS for oscillation damping [25]. BESS was suggested for mitigating SSR for heavy load fluctuations [26], while STATCOM equipped with BESS was used to damp out SSR by improving grid stiffness for a weak grid-connected wind farm [27]. The

**Table 1** Highlights of the current study compared to existing works

| Existing work | System type | SSR damping techniques | The measured input control signal | Analysis techniques | Stability addressed |
|---|---|---|---|---|---|
| 2019 [13] | Wind (PMSG) | UPFC-based-damping techniques | Locally measured | Complex torque coefficient method and time-domain analysis | Electromechanical mode |
| 2020 [21] | Wind(IG) | Pitch and resistance control technique | Locally measured | Eigenvalue + Time domain analysis | Electrical, electromechanical, and torsional mode |
| 2020 [20] | Wind(DFIG) | RSC-based damping techniques | Locally measured | Time domain analysis | Electrical mode |
| 2021 [18] | Wind(DFIG) | VGSTSMC | Locally measured | Time domain analysis | Electrical and electromechanical mode |
| 2021 [15] | Wind(IG) | Optimized (BFOA) STATCOM-based damping techniques | Locally measured | Eigenvalue + Time domain analysis | Electrical, electromechanical, and torsional mode |
| 2022 [11] | Conventional (Two non-identical multi-mass systems) | SSSC-based damping techniques | Locally measured | Eigenvalue + Time domain analysis | Electrical and torsional mode |
| 2022 [19] | Wind (PMSG) | Energy-shaping L2-gain controller | Locally measured | Eigenvalue + Time domain analysis | Electrical, electromechanical, and torsional mode |
| 2022 [17] | Wind (PMSG) | PLL-based damping techniques | Locally measured | Time domain analysis | Electrical mode |
| 2022 [14] | Wind (DFIG) | MMC-STATCOM-based damping techniques | Locally measured | Time domain analysis | Electrical mode |
| 2018 [22] | Conventional | SMEs based damping techniques | Locally measured | Time domain analysis | Torsional mode |
| 2020 [27] | Wind (PMSG) | STATCOM/BESS-based damping techniques | Locally measured | Time domain analysis | Electrical mode |
| 2021 [28] | Conventional | BESS + TCBR-based damping techniques | Locally measured | Time domain analysis | Torsional mode |
| This work | Wind (DFIG) | $BESSDC_L$ | WAMS techniques | Eigenvalue + Time domain analysis | Electrical, electromechanical, and torsional mode |

torsional oscillations in the shaft segments of steam turbo-generator units because of poor reclosure were minimized using a proposed fuzzy-based BESS [28]. In a WPP, an energy storage system with a bi-directional converter coupled to a DC connection was proposed, and an adaptive damping controller for a STATCOM employing a BESS was developed to reduce oscillations by controlling the active and reactive power of the grid side converter (GSC) [29].

However, current research has not adequately addressed the small-signal stability of a BESS-based damping controller in a variety of circumstances in a DFIG-based WPP. For the power system to operate safely and securely, small-signal stability is recognized as a key need. In contrast to earlier research, which only employs a locally recorded feedback signal as the input control signal (ICS) for SSR damping controller design, in this work a supplementary damping signal is established by taking the angular speed deviation as an ICS using WAMS. The benefit of adopting this technology is the ability to acquire real-time measurements from remote places, providing a more accurate picture of power system dynamics. The significance of this study in comparison to previous state-of-the-art research is shown in Table 1.

The motivation for to pursuing this research as can be deduced from Table 1 and includes:

1. Existing state-of-the-art techniques do not use BESS technology to alleviate the Sub-synchronous oscillations due to the SSR phenomenon in a DFIG-based WPP, nor do they analyze the small-signal stability.
2. Existing works use only locally measured feedback signals.
3. Generally, existing studies only address either the electrical or the torsional mode.

Thus, the critical contribution of this work is to design a BESS Damping Controller ($BESSDC_L$) and demonstrate its effectiveness in alleviating Sub-synchronous oscillations due to the SSR phenomenon in wind generation systems along with detailed mathematical modeling. The following are the specific contributions of the present research:

(a) Analysis of small-signal stability of the modified IEEE FBM of a DFIG-based WPP under various compensation and wind speed levels.
(b) To alleviate sub-synchronous oscillations, a $BESSDC_L$ is proposed and added to the busbar of a DFIG-based WPP with an FSC transmission line.
(c) A supplementary damping signal is developed considering angular speed deviations with the help of the WAMS technique.
(d) The efficacy of the proposed $BESSDC_L$ is authenticated using eigenvalue analysis as well as time-domain analysis at different compensation levels, wind speeds, and in different fault conditions.

The remaining part of the paper is organized as follows. The investigation of the study system, which is based on the IEEE FBM, and the analysis of the small-signal stability of the system are described in Sect. 2. Section 3 presents the alleviation of sub-synchronous oscillations by using BESS and discusses the detailed design of $BESSDC_L$. Section 4 presents the findings and discussions of the proposed system, while Sect. 5 presents the conclusions and observations.

## 2 Study system

As illustrated in Fig. 1, a modified IEEE FBM model-based study system is used to analyze the SSR phenomena. A 100 MW DFIG-based WPP is connected to the infinite bus system over a 161 kV fixed series compensated transmission line. The frequency of the generated voltage is 60 Hz [25], and the 100 MW WPP is composed of 67 wind turbines each rated at 1.5 MW. An analogous lumped machine model represents the aggregated behavior of a set of wind turbines, and it was validated by several recent studies in [20, 30] that wind farm aggregation is a good estimate for investigating system interconnection. This method has also been employed in system studies in [2, 9, 10, 23], which stated that "simulations of bulk system dynamics using a single machine equivalent are sufficient for most planning investigations". The Appendix contains the parameters for both the single and aggregated models.

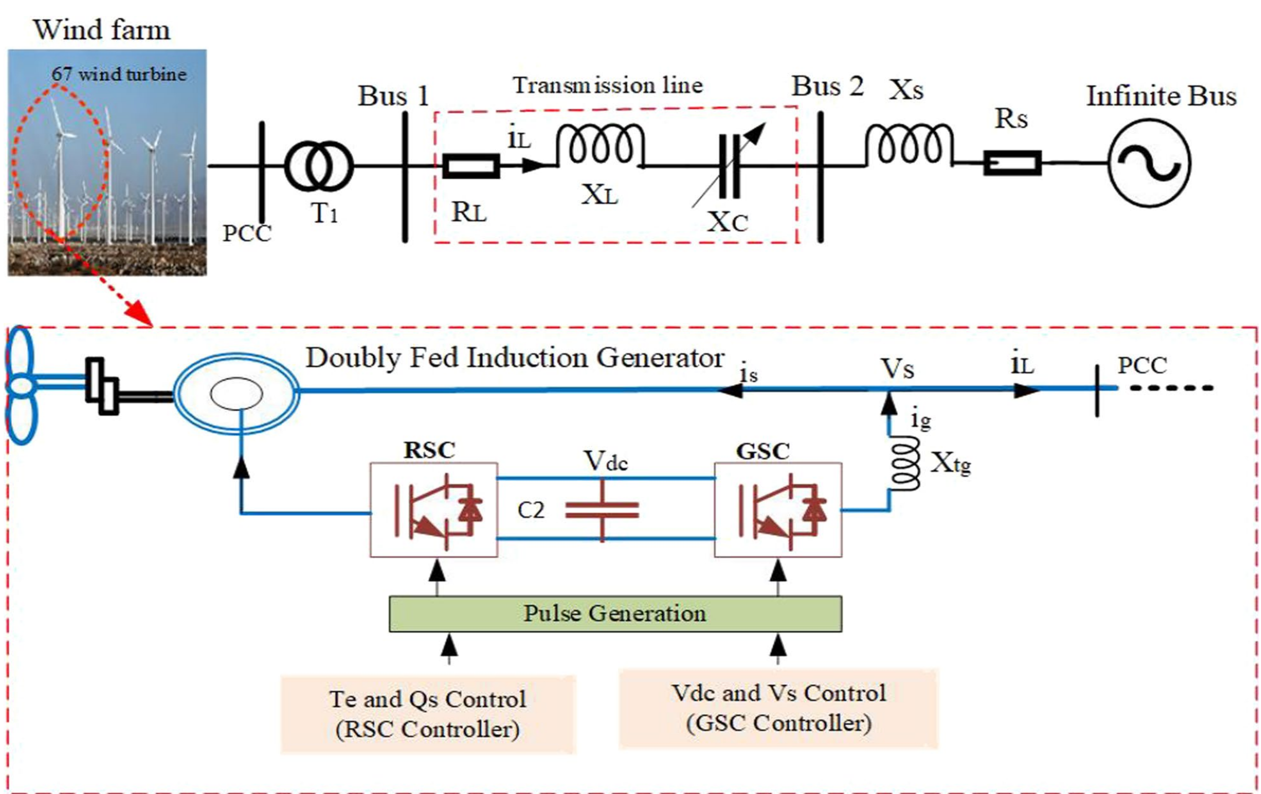


**Fig. 1** Modified IEEE FBM for SSR study [9, 23]

### 2.1 Small-signal modeling of the study system

#### 2.1.1 Modeling of wind turbine

The output of wind turbines, the relationship between mechanical torque and wind speed is expressed as [31, 32]:

$$Tm = \frac{\rho RAC_p V_{wi}^2}{2\lambda} \tag{1}$$

where ρ represents the air density ($kgm^{-3}$). The wind turbine rotor radius in meters (m) is represented by $R$, $A$ is the blade sweep area ($m^2$), $V_{wi}^2$ represents the speed of wind (m/s), and the blade power coefficient is $C_p$ and is expressed as:

$$C_p = 0.5\left(\frac{RC_f}{\lambda} - 0.022 * \theta - 2.0\right)e^{-0.255\left(\frac{RC_f}{\lambda}\right)} \tag{2}$$

and

$$\lambda = \frac{\Omega_m R}{V_{wi}} \tag{3}$$

where $\Omega_m$ denotes the mechanical angular velocity (rad/s).

#### 2.1.2 Modeling of shaft system

Torsional dynamics are commonly represented by a two-mass system when studying power system analysis. Considering that Mass-1 is a low-speed wind turbine shaft and Mass-2 represents the DFIG high-speed shaft system, this two-mass system is expressed in state-space representation as [32]:

$$\frac{d}{dt}\begin{pmatrix}\omega_t\\ \omega_r\\ T_g\end{pmatrix} = \begin{pmatrix}\frac{-D_t-D_{tg}}{2H_t} & \frac{D_{tg}}{2H_t} & \frac{-1}{2H_t}\\ \frac{D_{tg}}{2H_g} & \frac{-D_g-D_{tg}}{2H_g} & \frac{-1}{2H_g}\\ K_{tg}\omega_g & -K_{tg}\omega_e & 0\end{pmatrix}\begin{pmatrix}\omega_t\\ \omega_r\\ T_g\end{pmatrix} + \begin{pmatrix}\frac{T_m}{2H_t}\\ \frac{-T_e}{2H_t}\\ 0\end{pmatrix} \tag{4}$$

where the wind turbine, rotor speed of the DFIG, and internal torque of the model are represented by state variables $\omega_t$, $\omega_r$ and $T_g$, respectively. The mechanical and electromagnetic torques of the generator are represented by $T_m$ and $T_e$, respectively. The damping coefficient and inertia constants of the wind turbine are denoted by $D_t$ and $H_t$, respectively. $H_g$, $K_{tg}$ and $D_{tg}$ are,respectively, the inertia constant, damping coefficient, and shaft stiffness of the turbo-generator of the two-mass system. $T_e$ is expressed in terms of the d–q axes of the stator and rotor currents and air gap leakage fluxes of the DFIG as:

$$T_e = \psi_{qm} i_{dr} - \psi_{dm} i_{qr} \tag{5}$$

$$\psi_{qm} = X_m\left(i_{qs} + i_{qr}\right) \tag{6}$$

$$\psi_{dm} = X_m(i_{ds} + i_{dr}) \tag{7}$$

#### 2.1.3 Modeling of DFIG

A $6^{th}$-order dynamic model is used for the DFIG modeling [31, 33], described as:

$$\dot{X} = A_{DFIG} X_{DFIG} + B_{DFIG} U_{DFIG} \tag{8}$$

where state variables are denoted by $X_{DFIG}$. $U_{DFIG}$ denotes the DFIG inputs, $B_{DFIG}$ denotes the electrical parameter constants, and $A_{DFIG}$ denotes the constants of state variables, while there are:

$$X_{DFIG} = \left[i_{qs}; i_{ds}; i_{0s}; i_{qr}; i_{dr}; i_{0r}\right] \tag{9}$$

$$U_{DFIG} = \left[v_{qs}; v_{ds}; v_{0s}; v_{qr}; v_{dr}; v_{0r}\right] \tag{10}$$

The stator and rotor sides, direct, quadrature, and zero sequence components are denoted by the subscripts $r, s, q, d$ and 0, respectively. The parameters $i_{0s}$, $i_{0r}$, $v_{0s}$ and $v_{0r}$ are equal to zero because the system is balanced.

$A_{DFIG}$ and $B_{DFIG}$ are expressed as:

$$A_{DFIG} = -B_{DFIG}\begin{pmatrix} R_S & \frac{\omega_S}{\omega_b}X_S & 0 & 0 & \frac{\omega_S}{\omega_b}X_m & 0\\ -\frac{\omega_S}{\omega_b}X_S & R_S & 0 & -\frac{\omega_S}{\omega_b}X_m & 0 & 0\\ 0 & 0 & R_S & 0 & 0 & 0\\ 0 & \frac{\omega_S-\omega_r}{\omega_b}X_m & 0 & R_r & \frac{\omega_S-\omega_r}{\omega_b}X_r & 0\\ -\frac{\omega_S-\omega_r}{\omega_b}X_m & 0 & 0 & -\frac{\omega_S-\omega_r}{\omega_b}X_r & R_r & 0\\ 0 & 0 & 0 & 0 & 0 & R_r \end{pmatrix} \tag{11}$$

$$B_{DFIG} = -\omega_b\begin{pmatrix} X_S & 0 & 0 & X_m & 0 & 0\\ 0 & X_S & 0 & 0 & X_m & 0\\ 0 & 0 & X_{lS} & 0 & 0 & 0\\ X_m & 0 & 0 & X_r & 0 & 0\\ 0 & X_m & 0 & 0 & X_r & 0\\ 0 & 0 & 0 & 0 & 0 & X_{lr} \end{pmatrix}^{-1} \tag{12}$$

All variables and parameters are expressed in per-unit (pu) terms, except $\omega_b$, $\omega_r$, and $\omega_s$, which are in rad/s.

#### 2.1.4 Modeling of DC-link

The DC-link capacitor dynamic equations of the RSC and GSC are defined using a first-order model as [33, 34]:

$$C_{dc} V_{dc} \frac{dV_{dc}}{dt} = P_r - P_g \tag{13}$$

$$\mathrm{P}_r = \frac{1}{2}\left(v_{qr} i_{qr} + v_{dr} i_{dr}\right) \tag{14}$$

$$\mathrm{P}_g = \frac{1}{2}\left(v_{qg} i_{qg} + v_{dg} i_{dg}\right) \tag{15}$$

where $\mathrm{P}_r$ and $\mathrm{P}_g$ are the active power of the RSC and GSC, respectively. $V_{dc}$ is the actual DC voltage value, whereas $v_{qr}, i_{qr}, v_{dr}, i_{dr}, v_{qg}, i_{qg}, v_{dg}, i_{dg}$ are in pu terms.

#### 2.1.5 Modeling of a transmission line with fixed series compensation

Usually, the dynamic model of a power transmission line having FSC is ignored, but it is crucial for SSR analysis. The transmission line is characterized by an RLC series network and the synchronous reference frame is used to model a transmission line having fixed series compensation. Dynamic equations for each phase are stated as [33]:

$$R_L.i_L + L_L \frac{di_L}{dt} + v_C = v_s - V_B \tag{16}$$

$$C \frac{dv_C}{dt} = i_L \tag{17}$$

The state-space representation of the FSC power transmission line is:

$$\frac{d}{dt}\begin{pmatrix} i_{qL} \\ i_{dL} \\ v_{Cq} \\ v_{Cd} \end{pmatrix} = \omega_b \begin{pmatrix} -\frac{R_L}{X_L} & -\omega_e & -\frac{1}{X_L} & 0 \\ -\omega_e & -\frac{R_L}{X_L} & 0 & -\frac{1}{X_L} \\ X_C & 0 & 0 & -\omega_e \\ 0 & X_C & \omega_e & 0 \end{pmatrix} \begin{pmatrix} i_{qL} \\ i_{dL} \\ v_{Cq} \\ v_{Cd} \end{pmatrix} + \omega_b \begin{pmatrix} \frac{v_{qs}-V_{Bq}}{X_L} \\ \frac{v_{ds}-V_{Bd}}{X_L} \\ 0 \\ 0 \end{pmatrix} \tag{18}$$

where $i_{dL}$ and $i_{qL}$ are the direct and quadrature axes currents of the power transmission line. ($v_{Cq}$,$v_{Cd}$) and ($V_{Bq}$ ,$V_{Bd}$) are the quadrature and direct axes voltages across the capacitor and infinite bus, respectively. $\omega_b$ and $\omega_e$ are the base speed and synchronous reference speed, both equaling 377 rad/s or 1 pu.

#### 2.1.6 Overall system modeling without BESSDCL

Considering the overall system as an integration of the different subsystems [33], the overall system model is expressed as:

$$\left(\dot{X}\right) = \left(A_{sys}\right)\left(X_{sys}\right) + \left(B_{sys}\right)\left(U_{sys}\right) \tag{19}$$

$$\left(X_{sys}\right) = \left( X_{shaft} \; X_{DFIG} \; X_{tL} \; X_{dc} \right) \tag{20}$$

The system matrix of the integrated system model is given by:

$$\left(A_{sys}\right) = \begin{pmatrix} A_{shaft} & 0 & 0 & 0 \\ 0 & A_{DFIG} & 0 & 0 \\ 0 & 0 & X_{tL} & 0 \\ 0 & 0 & 0 & A_{dc} \end{pmatrix} \tag{21}$$

The above integrated subsystems communicate with each other through the state and control variables of the individual interconnected subsystem. The algebraic equations of $v_{ds}$, $v_{qs}$, $i_{ds}$ and $i_{qs}$ are used to link the controllers, and are expressed as:

$$v_{ds} = v_{dg} + X_{tg} i_{qg} \tag{22}$$

$$v_{qs} = v_{qg} + X_{tg} i_{dg} \tag{23}$$

$$i_{ds} = i_{dg} - i_{dl} \tag{24}$$

$$i_{qs} = i_{qg} - i_{ql} \tag{25}$$

Stator reactive power and developed torque are represented by:

$$T_g = X_m\left(i_{dr} i_{qs} - i_{ds} i_{qr}\right) \tag{26}$$

$$Q_s = \frac{1}{2}\left(v_{qs} i_{ds} - v_{ds} i_{qs}\right) \tag{27}$$

A state-space model is used to carry out the small-signal stability analysis of the study system. The eigenvalue analysis as well as time-domain analysis for the study system without damping controller are discussed in the results and discussion section.

## 3 Design of battery energy storage system damping controller ($BESSDC_L$)

A conventional BESS comprises a step-up coupling transformer, a passive inductive filter, a DC/AC power converter, and a battery bank [35]. Using the DC/AC power converter part of the BESS can alleviate the oscillations due to the SSR phenomenon using a Supplementary Damping Signal (SDS). Therefore, in the proposed system, to deal with the SSR phenomenon, a 200 kW battery energy storage system is added to Bus 2 of the 161 kV FSC power transmission line, as illustrated in Fig. 2. For designing the BESS-based damping controller, an SDS is added to the active power controller block of the converter in the BESS, and is triggered during transient conditions to dampen the oscillations. The Wide Area Measurement System (WAMS) and Phasor Measuring Units (PMU) are used in the proposed system to provide real-time information to the SDS.

### 3.1 Modeling of battery

Figure 3 depicts the electrical battery model and its electrical model parameters are calculated using [36]. In the first step, a specific capacity for the battery is determined.

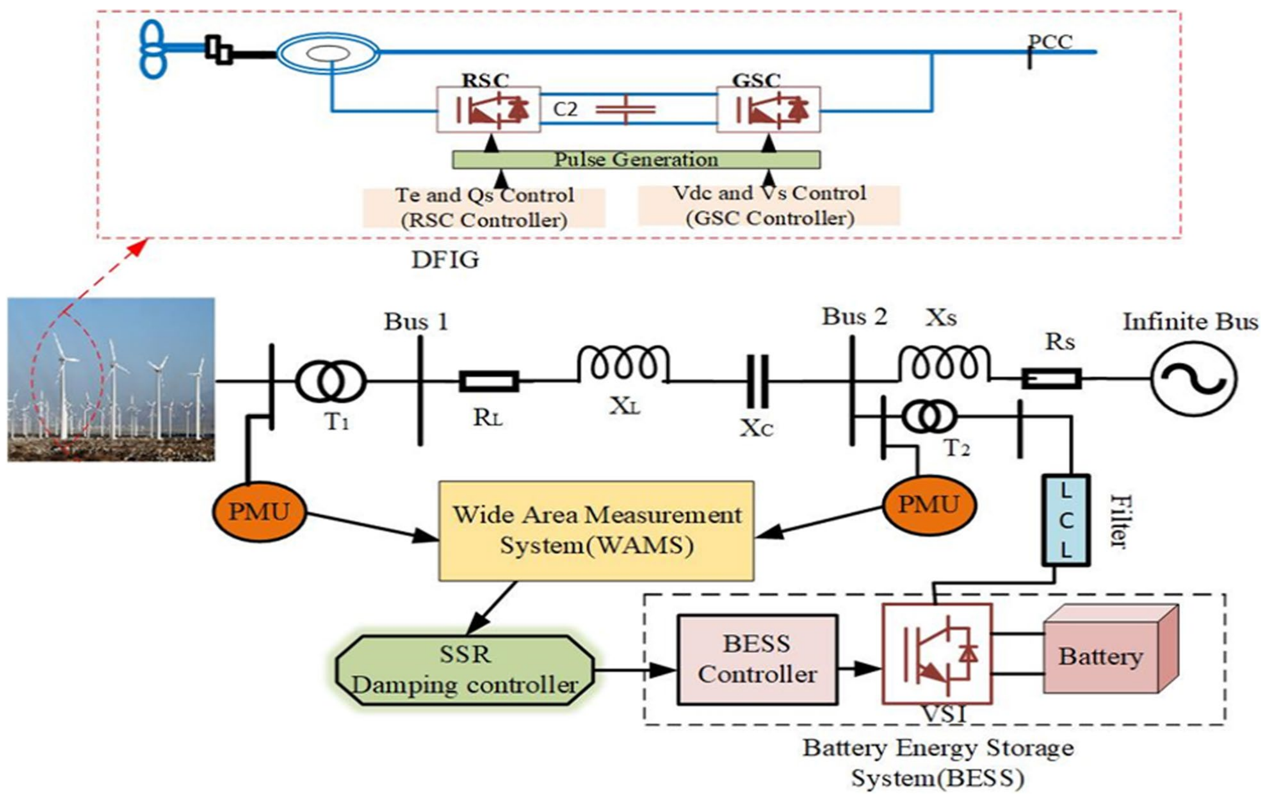


**Fig. 2** Proposed system model under study for the mitigation of SSR

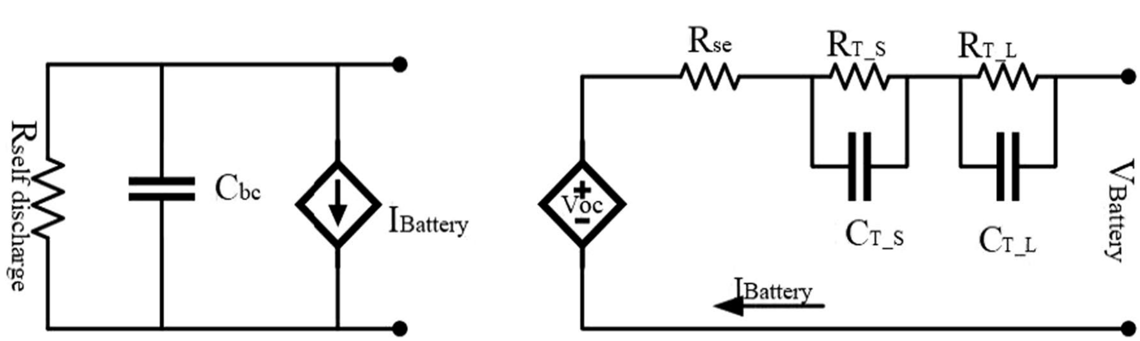


**Fig. 3** Electrical battery model [36]

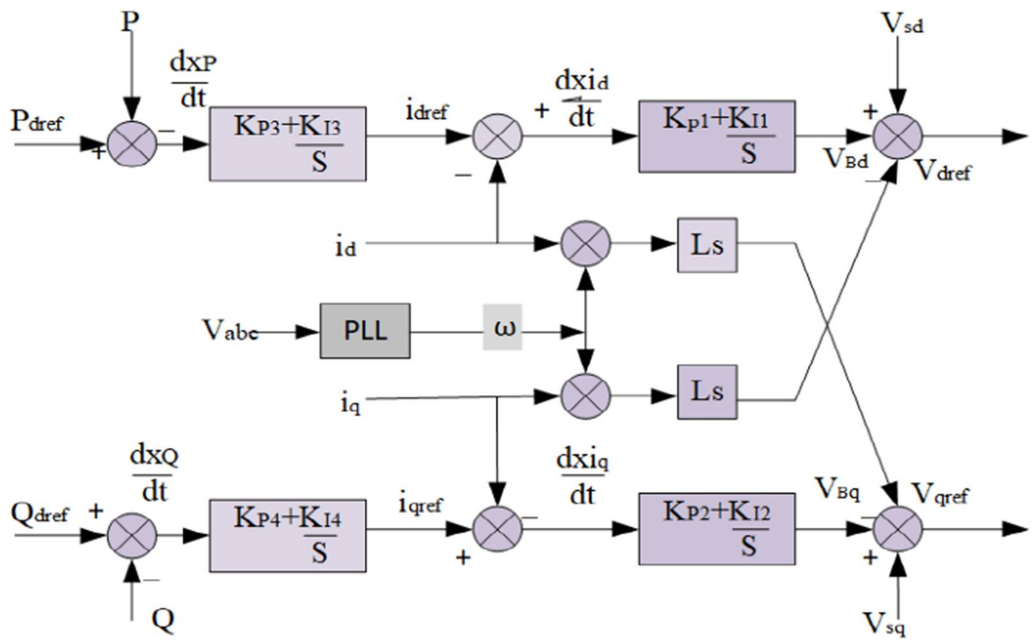


**Fig. 4** Traditional control strategy of BESS

Considering a 200 kW Li-ion battery as the energy storage system, the battery capacity can be computed as follows:

$$C_{bc} = Capacity(f_{1c})(f_{2T})3600 \tag{28}$$

where $C_{bc}$ is the capacity of the battery when completely charged, *Capacity* is denoted by nominal capacity in Ahr, the cycle number correction factor is denoted by $f_{1c}$ while the temperature-dependent correction factor is $f_{2T}$. The following parameters are taken as given in [36]:

$$V_{oc} = -1.030e^{-35Sbc} + 3.6 + 0.2Sbc - 0.1S_{bc}^2 + 0.3S_{bc}^3 \tag{29}$$

$$R_{se} = 0.15620e^{-24.37Sbc} + 0.0744 \tag{30}$$

$$R_{T\_L} = 6.6030e^{-155.2Sbc} + 0.0498 \tag{31}$$

$$C_{T\_L} = 6065.0e^{-27.12Sbc} + 4475.0 \tag{32}$$

$$R_{T\_S} = 0.32080e^{-29.14Sbc} + 0.0466 \tag{33}$$

$$C_{T\_S} = -752.90e^{-13.51Sbc} + 703.60 \tag{34}$$

where $V_{oc}$ is the battery voltage in the open circuit condition, Sbc is the battery cell's state of charge, and $R_{se}$ is the resistor in series. $R_{T\_S}$ and $R_{T\_L}$ are the short and long transient resistors, respectively, while the short and long transient capacitors are $C_{T\_S}$ and $C_{T\_L}$, respectively.

The generated battery energy is then sent to the grid via a three-phase converter. As demonstrated in Fig. 4, the BESS employs constant power control and PQ control.

The BESS grid voltages are $V_{sa}$, $V_{sb}$ and $V_{sc}$, and their *dq* axes components are $V_{sd}$ and $V_{sq}$. The BESS controller output voltages are $V_{Ba}$, $V_{Bb}$ and $V_{Bc}$, and their *dq* axes components are $V_{Bd}$ and $V_{Bq}$ The BESS output currents are $i_a$, $i_b$ and $i_c$, and their *dq* axes components are $i_d$ and $i_q$. The inductance of the BESS grid line is $Ls$ and ω represents the angular synchronous frequency. The DC side capacitor, voltage, and current are referred to as $C_{dcB}$, $V_{dcB}$ and $i_{dcB}$, respectively. Considering $i_d$, $i_q$, $x_Q$, $x_{id}$, $x_P$, $x_{iq}$ and $V_{abc}$ as the state variables, the small-signal model for the BESS can be configured as follows [24, 27–29]:

Transmission line state space equations:

$$\frac{di_d}{dt} = \frac{\omega}{L_s}\left(V_{dref} + L_s i_q\right) \tag{35}$$

$$\frac{di_q}{dt} = \frac{\omega}{L_s}\left(V_{qref} + L_s i_d\right) \tag{36}$$

Controller state space equations:

$$\frac{dx_p}{dt} = P_{dref} - \left(V_{Sq} i_d - V_{Sd} i_q\right) \tag{37}$$

$$\frac{dx_{id}}{dt} = K_p\left(P_{dref} - \left(V_{Sq} i_d - V_{Sd} i_q\right) + K_{I1}\left(x_p - i_d\right)\right) \tag{38}$$

$$\frac{dx_Q}{dt} = Q_{dref} - \left(V_{Sd}i_d - V_{Sq}i_q\right) \tag{39}$$

$$\frac{dx_{iq}}{dt} = K_{p4}\left(Q_{dref} - \left(V_{Sd}i_d - V_{Sq}i_q\right) + K_{I4}\left(x_Q - i_q\right)\right) \tag{40}$$

DC capacitor state space equation:

$$\frac{dV_{dcB}}{dt} = \frac{\omega}{C_{dcB}V_{dcB}}\left(V_{Bd}i_{Bd} + V_{Bq}i_{Bq}\right) \tag{41}$$

For the model analysis, the entire system models are represented by:

$$\dot{X} = f(X, U) \tag{42}$$

whereas $X = \left(X_{shaft}\ X_{DFIG}\ X_{tl}\ X_{dc}\ X_{BESS}\right)$ is assembled in MATLAB/Simulink to obtain the eigenvalue analysis.

### 3.2 Control system of BESSDCL

The configuration of the Voltage Source converter (VSC)-based BESS is used to mitigate the sub-synchronous oscillation in the WPP. The major component of the BESS is the inverter controller. Figure 5 depicts the schematic diagram of a distinctive grid-connected VSC-based BESS [37]. There are four levels of control involved in the developed controller, including SDS, power controller block, inner current controller block, and a Pulse Width Modulation (PWM) unit. This paper considers WAMS data to obtain the angular speed deviation as the input for the SDS. It is denoted by U and is supplemented by the active power of the power controller block as depicted in Fig. 5, in order to dampen the sub-synchronous oscillations. The output of the primary power controller block is to provide $i_{dref}$ and $i_{qref}$ reference currents to the inner current-controller block, which regulates the AC side currents of the VSC [38]. First, $i_d$ and $i_q$ are compared to $i_{dref}$ and $i_{qref}$, respectively, as shown in Fig. 5. The decoupling of the feed-forward signals is used to improve the outputs of the Proportional-integral (PI) controllers, which process error signals. For the PI parameter tuning a systematic trial-and-error approach is used to produce fast step response and short settling time with less than 10% overshoot. The inner controller block provides the *dq* reference voltages, which are translated to *abc* reference frame to be fed into the PWM unit to generate pulse signals. The LCL filter is used in the system, and is interconnected through a coupling transformer, to minimize the ripples at the AC side of the VSC so that the system can deliver low distorted current and voltage at the output [39].

### 3.3 Design of the supplementary damping signal

Figure 6 illustrates the configuration of the SDS, whose objective is to provide additional damping. This can be achieved without reducing the synchronizing torque. A washout, two lead-lag compensators, a gain as well as a limiter block comprise the SDS design technique in this

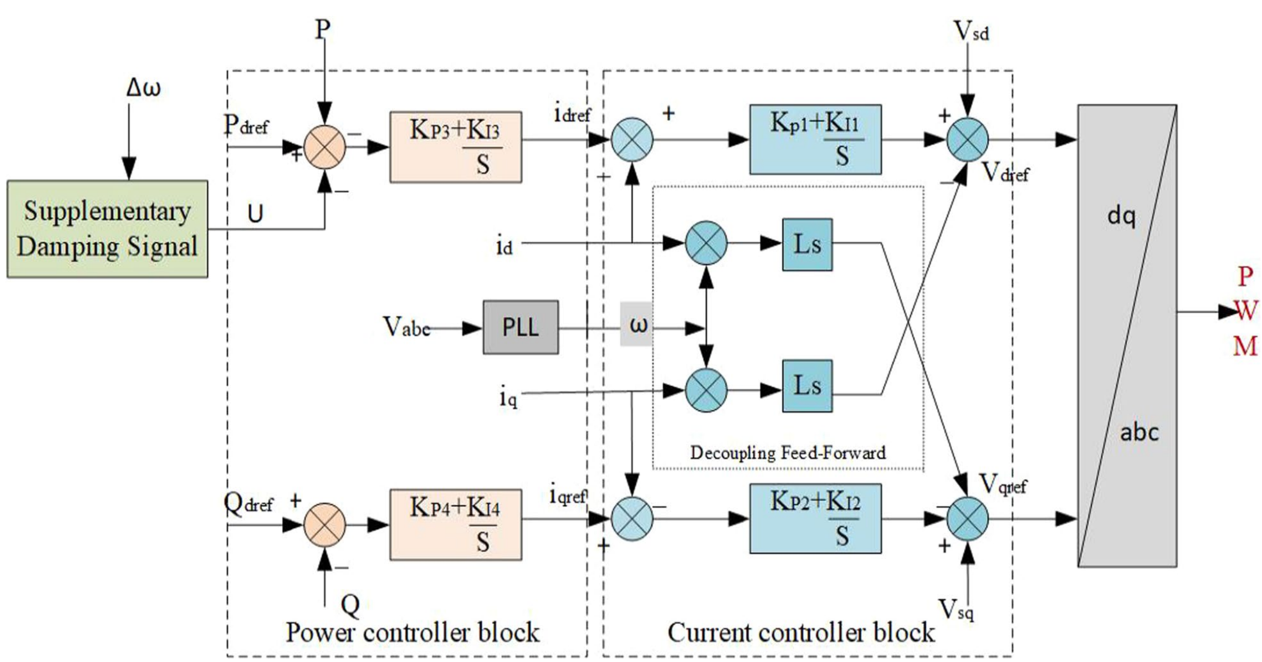


**Fig. 5** BESSDC$_L$ controller for the SSR mitigation

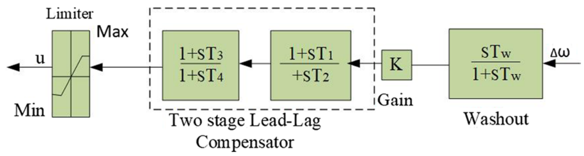


**Fig. 6** Supplementary damping signal

**Table 2** Parameters for the supplementary damping signal

| Parameter | $K$ | $T_W$ | $T_1$ | $T_2$ | $T_3$ | $T_4$ | Min and Max |
|---|---|---|---|---|---|---|---|
| Value | 1.38 | 10 | 0.1 | 0.01 | 0.4 | 2 | $\mp 0.1$ |

study, as illustrated in Fig. 6 [40, 41]. The design of the SDS transfer function is defined as:

$$SDS(s) = \frac{sT_W}{1 + sT_W} T(s) \tag{43}$$

and the transfer function of the lead-lag compensator T(s) is defined as:

$$T(s) = \frac{K(1 + sT_1)(1 + sT_3)}{(1 + sT_2)(1 + sT_4)} \tag{44}$$

whereas $T_W$ denotes the washout time constant, while the washout block acts as a high pass filter to prevent DC and low-frequency components. $K$ represents the gain of the damping signal. This determines the strength of the damping. A higher gain will provide stronger damping, but may also introduce instability. The gain should be carefully tuned to achieve the desired damping effect without introducing instability. $T_1$, $T_3$, $T_2$, and $T_4$ are the time constants of the two-stage lead-lag compensator block. The compensator consists of a lead network and a lag network, each of which contributes to the overall phase shift of the system. The phase shift of the lead network should be chosen to align with the frequency of the sub-synchronous oscillation, while the phase shift of the lag network should be chosen to provide additional damping. The compensator parameters are tuned based on the eigenvalues of the system matrix and their locations in the complex plane along with systematic trial-and-error methods to achieve the desired level of damping.

The number of unknown parameters is six and they need to be determined. The number of algebraic equations must equal the number of the unknown controller parameters according to the model theory. The required parameters for the controller may be obtained simply by solving the set of linearized algebraic equations of (43). Therefore, the parameters of the controller are determined by substituting the desired eigenvalues corresponding to modes 3, 4, and 6 to the closed loop system characteristics equation:

$$|sI - (A + B.SDS(s)C)| = 0 \tag{45}$$

where I is the identity matrix of the same dimension as A.

To obtain optimal parameters, a systematic trial-and-error procedure is used to tune the SDS parameters to produce a fast step response, less settling time, and less than 10% overshoot to minimize the impact on system stability and transient response efficiently. The conditions that should be followed are $T_1 > T_2$ and $T_3 < T_4$. The obtained optimal parameters are shown in Table 2.

The angular speed deviation signal is used as the input control signal in the proposed system, and the SDS input is designed to alleviate SSR while WAMS is used to measure the frequency deviation of the generator. As shown in Fig. 5, the SDS output is added to the battery controller, and this regulates the BESS's reference active power generation.

### 3.3.1 Input control signal

The major challenge of selecting a speed deviation as an Input Control Signal (ICS) is to capture the angular speed deviation of a generator and transmit it to the other components of the system that are far away from the generator. The advance in technologies such as WAMS, PMU, and communication networks allows obtaining the most accurate and real-time data on the dynamic parameters of a complex power system [42, 43]. At the same time, it is essential to have real-time data for the parameters such as frequency, voltage, and current from the generating station to the transmission system. However, this paper focuses on using speed deviation as an ICS for designing a damping controller to mitigate the SSR. Generally, PMUs are installed to measure the voltage and frequency at a busbar. These can be transmitted to other substations. The installed PMU captures the data regarding current, voltage, frequency, and other parameters at regular intervals on a sample basis, and the data are stored in data concentrators. Each PMU is generally time synched with the GPS devices, and the data stored in the form of samples are time-stamped and can be used for the analysis of complex power systems. The samples taken from the PMU devices should be in milliseconds so that exact analysis can be done at the remote end for frequency deviations observed in the synchronous generator [44]. The time-stamped data of analog parameters stored in the data concentrator are transferred to the remote end with the support of the WAMS network. The role of WAMS is to monitor the data transmission from PMUs to the central controller, ensuring reliable data transfer from several stations to the computation center. This paper analyzes the BESS technology controller to dampen the SSR oscillations, while WAMS serves the purpose of providing real-time data of angular speed deviation at the synchronous generator to the controller input installed in BESS technology at the remote end busbar unit. The details and arguments for employing WAMS to capture rotor speed data have been described in [36] and are thus not described further in this paper.

## 4 Results and discussion

To further analyze the small-signal stability, the eigenvalue method is used. To validate the eigenvalues, time domain analysis is also carried out in this section using MATLAB/Simulink.

### 4.1 Eigenvalue analysis without damping controller

To study the small-signal stability of a dynamic system, the eigenvalue method is a fundamental and effective methodology. In this method, the order of the system matrix decides the set of eigenvalues, while the analysis of eigenvalues reveals the stability of the system. The system is unstable if any real components of the eigenvalues are positive, and stable if the real parts of the eigenvalues are negative. The oscillating frequencies are decided by the imaginary parts of the eigenvalues. The eigenvalue analysis exhibits six unstable modes of oscillatory behavior when applied in the above linearized study system without any damping controller. Table 3 displays the set of eigenvalues of the six modes at an FSC level of 50% and 7 m/s wind speed. Mode 1 and Mode 2 show high frequencies with a super-synchronous phenomenon, and are always stable.

Mode 3 belongs to the sub-synchronous frequency range and is not stable in this operating state. As can be seen from Table 4, the system may become progressively unstable at increasing series compensation level. Mode 4 is the electromechanical mode due to the dynamics of electromechanical systems, while the remaining Modes 5 and 6 are the torsional modes. As the series compensation level is increased, it can be seen from Table 4 that the positive real parts of the eigenvalues are increasing. This shows that the system is tending towards instability. On the other hand, the real parts of the eigenvalues are decreased when the speed of the wind is increased. This shows that at higher wind speed, the system becomes more stable. The time-domain simulation of the same system is provided in the following subsections.

**Table 3** Eigenvalues of the study system model with 50% fsc level and 7 m/s wind speed

| Modes | Eigenvalue | Frequency (Hz) | Description |
|---|---|---|---|
| Mode 1 | $-1790 \pm j889$ | 141 | Very high frequency |
| Mode 2 | $-19.2 \pm j568.2$ | 90.4 | Super-synchronous |
| Mode 3 | $1.6 \pm j187.8$ | 29.9 | SSR |
| Mode 4 | $-0.63 \pm j18.8$ | 2.86 | Electromechanical |
| Mode 5 | $-52.4 \pm j7.9$ | 1.25 | Torsional mode |
| Mode 6 | $-6.41 \pm j8.6$ | 1.36 | Torsional mode |

### 4.2 Small-signal model validation

In order to verify the small-signal model of the proposed study system, a detailed electromagnetic transient model is built in the MATLAB/Simulink simulation platform. Accordingly, IEEE's first benchmark model is simulated for a wind speed of 7 m/s and a 50% series compensated transmission line. Figures 7, 8 and 9 show the simulation results. The dynamic behavior of the active,

**Table 4** Mode-3 eigenvalue at varying percentage of series compensation and wind speed

| Compensation | Wind speed (m/s) | Mode 3 | |
|---|---|---|---|
| | | Eigenvalue | Frequency (Hz) |
| 40% | 7 | $0.01 \pm j207$ | 32.96 |
| | 9 | $-0.04 \pm j206.9$ | 32.94 |
| | 11 | $-0.12 \pm j206.8$ | 32.92 |
| 50% | 7 | $1.66 \pm j187.8$ | 29.90 |
| | 9 | $1.56 \pm j187.7$ | 29.87 |
| | 11 | $1.43 \pm j187.5$ | 29.84 |
| 60% | 7 | $3.26 \pm j170.9$ | 27.25 |
| | 9 | $3.15 \pm j170.7$ | 27.14 |
| | 11 | $2.95 \pm j170.4$ | 27.18 |

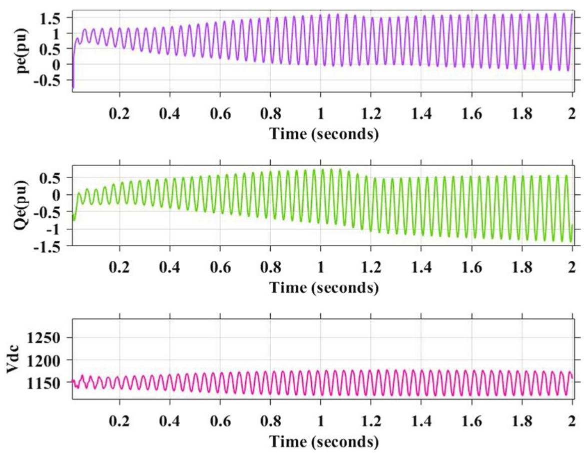


**Fig. 7** Dynamic behavior of the active power (pe), reactive power (Qe), and DC-link voltage (Vdc) of the DFIG at a FSC of 50%

reactive, and DC-link voltage of the DFIG are shown in Fig. 7, and the waveforms show undamped oscillations at a 50% compensation level. The eigenvalues in Table 3 show that Mode 3 is unstable at a wind speed of 7 m/s and 50% compensation. The obtained eigenvalues of Mode 3 at varying series compensation and wind speed are shown in Table 4. The frequencies of Mode 3 are 32.94 Hz, 29.87 Hz, and 27.14 Hz at series compensations of 40%, 50%, and 60%, respectively. For the validation of the results seen in the eigenvalue analysis, the time-domain analysis and its Fast Fourier Transform (FFT) are analyzed. Figure 8 shows the dynamic behaviors of the electromagnetic torque (Te) at 40%, 50%, and 60% compensation levels at 9 m/s wind speed, and the FFT analysis results. Figure 9 shows the dynamic behavior of the electromagnetic torque (Te) at 7 m/s, 9 m/s, and 11 m/s wind speed at 50% series compensation, with the corresponding FFT analysis. As seen, the FFT analysis of the time domain signals has the same frequencies as the eigenvalue analysis shown in Table 4.

### 4.3 Eigenvalue analysis with BESSDCL

The proposed $BESSDC_L$ is applied in the benchmark model to study the efficacy of the proposed damping controller by eigenvalue analysis. This was performed without the damping controller in the previous section with

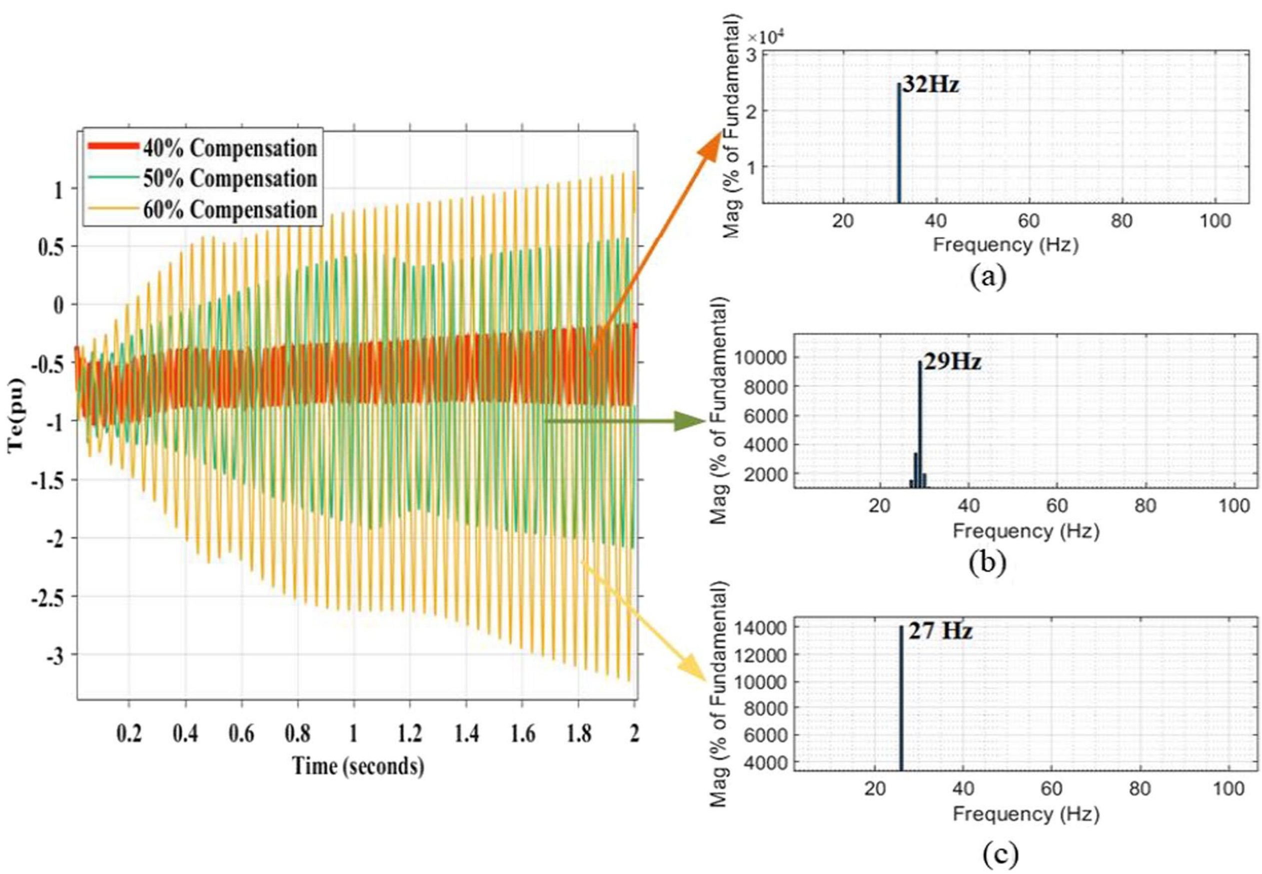


**Fig. 8** Dynamic behavior of the electromagnetic torque (Te) of 40%, 50%, and 60% compensation level at 9 m/s wind speed: **a** FFT analysis for 40% series compensation; **b** 50% series compensation; and **c** 60% series compensation

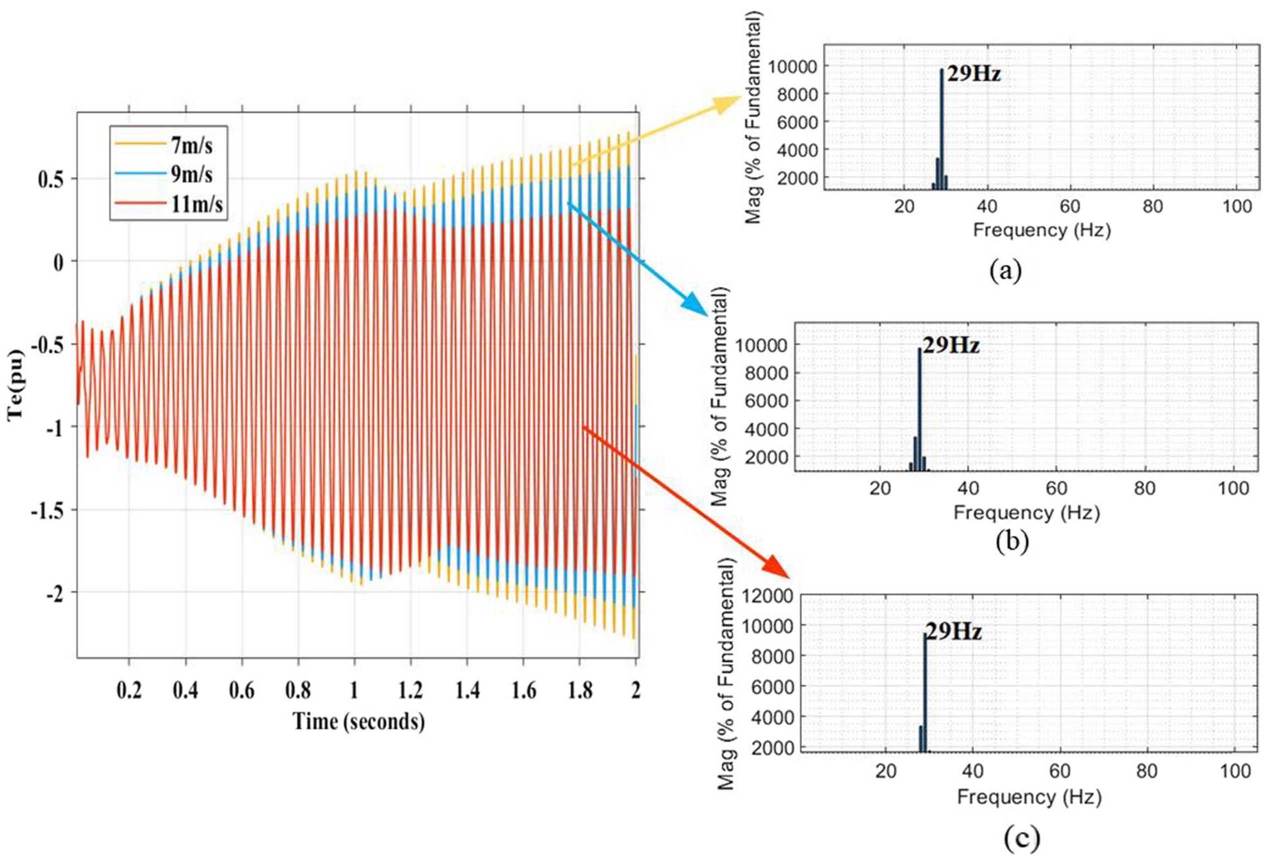


**Fig. 9** Dynamic behavior of the electromagnetic torque (Te) of 7 m/s, 9 m/s and 11 m/s wind speed at 50% series compensation: **a** FFT analysis for 7 m/s wind speed; **b** 9 m/s wind speed; and **c** 11 m/s wind speed

six modes of oscillations obtained. Mode 3 is undamped and is an unstable mode at sub-synchronous frequency. Table 5 displays the eigenvalues of the study system with a BESSDC$_L$. This shows that all modes are stable even when the series compensation is set to 50%. Table 6 displays the eigenvalues of the study system with the BESSDC$_L$ at different compensation levels and wind speeds, and it is found that even after increasing the compensation level, the controller is capable of providing positive damping and all the resultant modes are in a stable condition.

**Table 5** Eigenvalues of the study system model with BESSDC$_L$ AT 50% FSC transmission line and 7 m/s wind speed±

| Modes | Eigenvalue | Frequency(Hz) |
|---|---|---|
| Mode 1 | − 17.93 ± j887 | 141.2 |
| Mode 2 | − 16.2 ± j524.5 | 83.51 |
| Mode 3 | − 1.5 ± j229.2 | 36.49 |
| Mode 4 | − 49.4 ± j10.9 | 1.73 |
| Mode 5 | − 0.63 ± j18.8 | 2.99 |
| Mode 6 | − 4.5 ± j10.2 | 1.62 |

**Table 6** Mode-3 eigenvalue at varying series compensation level and wind speed with BESSDC$_L$

| Compensation | Wind speed (m/s) | Mode 3 | |
|---|---|---|---|
| | | Eigenvalue | Frequency(Hz) |
| 40% | 7 | − 3.0 ± j255.9 | 40.74 |
| | 9 | − 3.04 ± j255.84 | 40.74 |
| | 11 | − 3.09 ± j255.8 | 40.73 |
| 50% | 7 | − 1.5 ± j229.23 | 36.50 |
| | 9 | − 1.54 ± j229.2 | 36.49 |
| | 11 | − 1.6 ± j229.1 | 36.48 |
| 60% | 7 | − 1.04 ± j207 | 32.96 |
| | 9 | − 1.09 ± j206.8 | 32.92 |
| | 11 | − 1.16 ± j206.82 | 32.93 |

### 4.4 Time-domain analysis for BESSDCL

It has been shown that BESSDC$_L$ equipped with an SDS composed of the angular speed deviation can damp out oscillations due to SSR. To enhance BESSDCL performance, further time-domain simulations are carried out

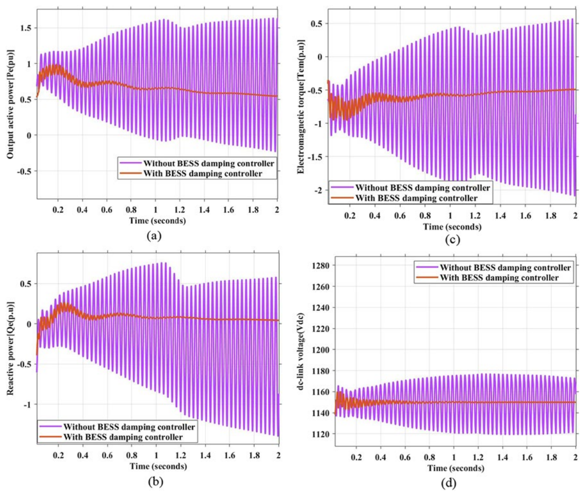


**Fig. 10** Time responses of the system comprising DFIG with and without the proposed BESSDC$_L$: **a** output active power, **b** reactive power, **c** electromagnetic torque, **d** DC-link voltage

in MATLAB/Simulink. The baseline scenario is considered at a wind speed of 9 m/s and 50% FSC, and the IEEE FBM model is used to analyze the performance of the proposed damping controller. The equivalent model is the same as shown in Fig. 2 with the same parameter as illustrated in the Appendix.

### 4.4.1 Damping performance of the BESSDCL

The simulation is done for the baseline scenario to verify that the BESSDC$_L$ can damp out the undamped oscillations due to SSR. Figure 10 shows the system dynamic responses for the DFIG output active power, reactive output power, electromagnetic torque, and DC-link voltage with and without the proposed BESS damping controller. As seen, active power of 0.53 pu is achieved with 9 m/s wind speed, while the power factor is adjusted to 1 at the stator and grid side terminal, ensuring that the expected reactive power for the DFIG for steady-state conditions is zero. The DC-link voltage reference is 1150 V. Figure 10 shows that the system responses are stable when using the proposed damping strategy based on the BESS. Taking the case without using BESSDC$_L$, due to SSR, the rotor circuit action on damping SSR is negative. Hence, undamped sub-synchronous oscillations are generated on DFIG responses resulting in an unstable system.

### 4.4.2 Robustness of the BESSDCL

The simulation for the baseline scenario is further expanded to validate the robustness of the proposed BESSDC$_L$ in mitigating the sub-synchronous oscillations due to SSR in three cases as follows: (i) varying fixed series compensation levels; (ii) varying wind speeds; and (iii) three-phase fault condition.

*4.4.2.1 Varying fixed series compensation levels* The baseline scenario is simulated at 50% and then 60% of FSC while other parameters are fixed. The system damping is directly related to the FSC level, and the performance of the pro-

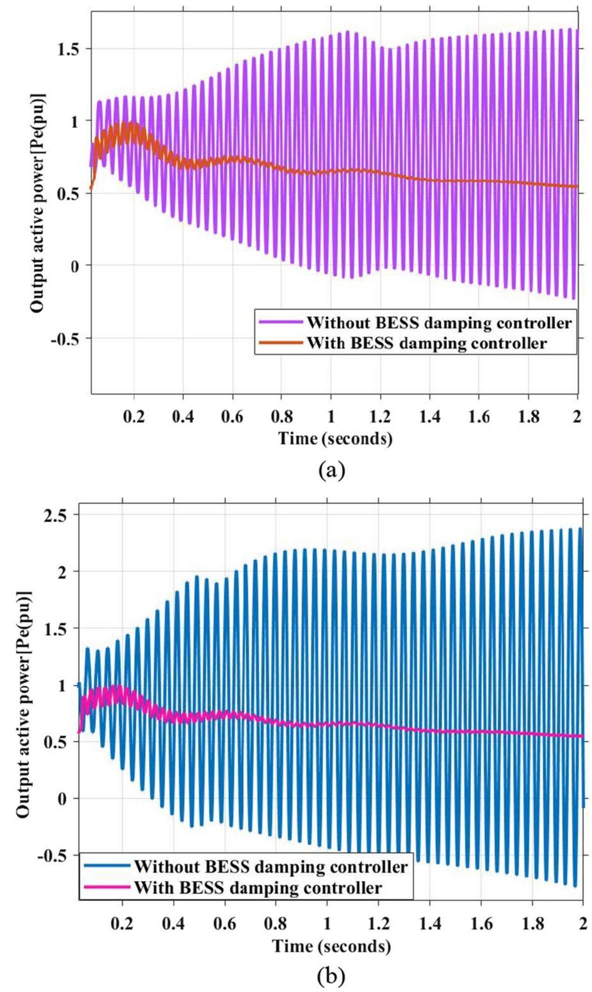


**Fig. 11** The output active power of DFIG with and without BESSDC$_L$ at: **a** 50% series compensation and 9 m/s wind speed; **b** 60% series compensation at 9 m/s wind speed

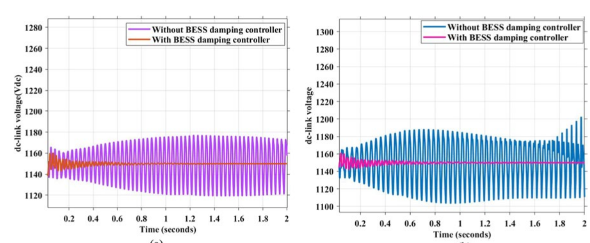


**Fig. 12** DC-link voltage with and without BESSDC$_L$ at: **a** 50% series compensation and 9 m/s wind speed; **b** 60% series compensation at 9 m/s wind speed

posed BESSDC$_L$ at various series compensation levels is validated. This is equivalent to the performance of BESSDC$_L$ in various damping conditions. As depicted in Fig. 8, when the level of FSC increases, the amplitude of the undamped oscillation increases, and eventually, the system becomes unstable. The amplitude of the output power oscillation is reduced when BESSDC$_L$ is added to the system even when increasing the FSC level from 50 to 60%. Figure 11 depicts the active power of the DFIG with and without BESSDC$_L$, while Fig. 12 displays the DC-link voltage.

*4.4.2.2 Varying wind speeds* The baseline scenario is simulated at a wind speed of 11 m/s and 7 m/s rather than 9 m/s, whereas other parameters are fixed. Figure 13 depicts the active power output of the DFIG with and without BESSDC$_L$ at different wind speeds. It shows that after using the damping controller the undamped oscillations are damped out. The results demonstrate that the proposed damping controller is proficient in damping out oscillations at different wind speeds. Correspondingly, Fig. 14 depicts the DC-link voltages of the DFIG with and without BESSDC$_L$.

*4.4.2.3 Three-phase fault condition* In an electrical power system, three-phase faults are of severe concern and the disturbances can be very serious. Consequently, it is essential to test the proposed damping controller's suppression capability during three-phase faults. The baseline scenario is simulated at an FSC level of 50% and a wind speed of 9 m/s, and the series compensating capacitance is activated before the fault. The fault is introduced at 0.2 s and eliminated at 0.4 s. During the fault, the active power declines almost to zero, as depicted in Fig. 15. Without the BESSDC$_L$, the active power generated by the DFIG experiences severe sub-synchronous undamped oscillation and consequently the system loses stability. When the BESSDC$_L$ is activated at 1 s, the oscillation converges and the system regains stability, as seen in Fig. 16. Figure 17 shows the DC-link voltage of the DFIG in the three-phase fault condition. The simulation results show that the BESSDC$_L$ has excellent restraining effect even in the worst-case three-phase fault scenario.

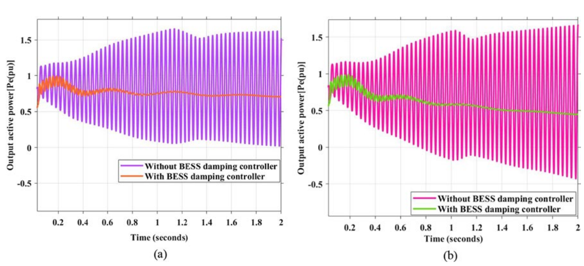


**Fig. 13** The output active power of DFIG with and without BESSDC$_L$ at: **a** 7 m/s wind speed; **b** 11 m/s wind speed at 50% series compensation

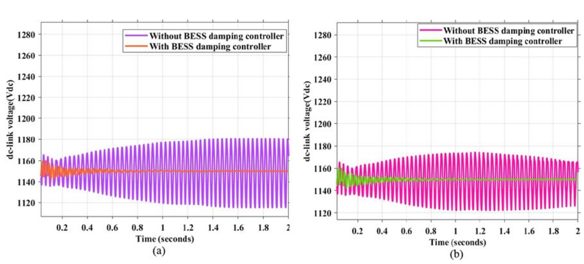


**Fig. 14** DC-link voltage with and without BESSDC$_L$ at 50% series compensation and: **a** 7 m/s wind speed; **b** 9 m/s wind speed

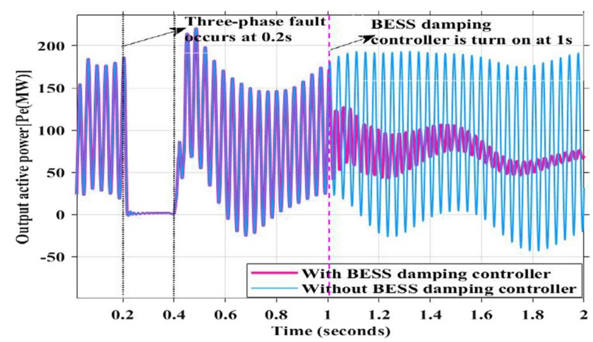


**Fig. 15** The output active power without and with BESSDC$_L$ under three-phase fault condition

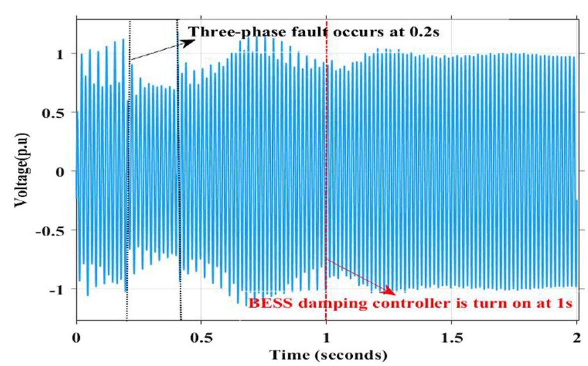


**Fig. 16** The phase output voltage of DFIG at bus 1

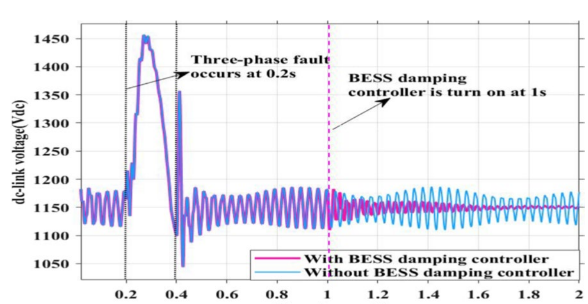


**Fig. 17** DC-link voltage without and with BESSDC$_L$ under three-phase fault condition

## 5 Conclusion

To investigate the SSR phenomena, a detailed mathematical model of a 100 MW DFIG-based WPP interconnected to an infinite bus with an FSC power transmission line has been developed based on the IEEE FBM. With the help of eigenvalue analysis, the several modes of oscillation in the overall system, i.e., electrical, electromechanical, and torsional modes, are obtained. The estimated eigenvalues of the overall study system for different operating conditions are used to identify the stable and unstable modes of frequencies and unstable SSR modes. Two cases are investigated for small-signal stability, including varying compensation levels and wind speeds. To alleviate the sub-synchronous oscillations due to SSR and enhance power system operation, a $BESSDC_L$ equipped with a supplementary damping signal composed of the angular speed deviation is proposed to damp out oscillations in wind-integrated power grids effectively even after increasing the series compensation level from 50 to 60%. In the proposed method, WAMS data is used to obtain angular speed deviation to be used as the input control signal. To validate the performance of the proposed controller, eigenvalue analysis and time-domain simulation are carried out using MATLAB/Simulink. The dynamic behavior of the electromagnetic torque, active power, reactive power, and DC-link voltage of the DFIG for various compensation levels, wind speeds, and three-phase fault condition are investigated in this paper. The results show that the proposed $BESSDC_L$ is capable of damping out the oscillations in a very effective manner. Moreover, since the proposed $BESSDC_L$-based damping controller does not need the modification of other power system controllers or the detection of harmonics, it can easily be applied to various scenarios for minimizing sub-synchronous oscillations caused by the SSR.

## Appendix

See Tables 7, 8 and 9

**Table 7** Parameters of the DFIG

| Parameter | Rating | |
|---|---|---|
| | Individual | Aggregated |
| Rated power | 1.5 MW | 100 MW |
| Rated voltage | 575 V | 575 V |
| Rated frequency | 60 Hz | 60 Hz |
| $R_S$ | 0.023 | 0.023 |
| $X_{lS}$ | 0.18 | 0.18 |
| $R_r$ | 0.016 | 0.016 |
| $X_{lr}$ | 0.16 | 0.16 |
| $X_M$ | 2.9 | 2.9 |
| DC-link voltage | 1150 V | 1150 V |
| DC-link capacitor | 10,000 μF | 67*10,000 μF |

**Table 8** Parameters of drive train

| Parameter | Rating |
|---|---|
| $H_t$ | 4.32 s |
| $H_g$ | 0.685 s |
| $D_t$ | 0 |
| $D_g$ | 0 |
| $D_{tg}$ | 1.5 pu |
| $K_{tg}$ | 1.11 |

**Table 9** Parameters of transmission line

| Parameter | Rating |
|---|---|
| Transformer Ratio | 575 V / 161 kV |
| Base power | 100 MVA |
| $R_L$ | 0.02 |
| $X_L$ | 0.50 |
| $X_C$ at 50% compensation | 64.8 Ω |
| $X_T$ | 0.14 |
| $X_{sys}$ | 0.060 |

**Abbreviations**

SSR Sub-synchronous resonance
PMSG Permanent magnetic synchronous generator
WPP Wind power plant
BESS Battery energy storage system
FSC Fixed series compensation
GSC Grid side converter
ICS Input control signal
$BESSDC_L$ Battery energy storage system damping controller
DFIG Doubly-fed induction generator
STATCOM Static synchronous compensator
RSC Rotor side converter
SDS Supplementary damping signal
WAMS Wide area measurements system
PMU Phase measurement unit
FBM First benchmark model

**Acknowledgements**
NA

**Author contributions**
NV: Original draft preparation, conceptualization, methodology, software, data curation, formal analysis. Dr. NK: Supervision, reviewing, and editing. Dr. RK: Conceptualization, methodology, original draft preparation, supervision, formal analysis, reviewing, and editing, validation.

**Funding**
No funding has been received for this work.

**Availability of data and materials**
Data sharing not applicable to this article as no datasets were generated or analysed during the current study.

## Declarations

**Competing interests**
The authors declare that they have no known competing financial interests or personal relationships that could have appeared to influence the work reported in this paper.

Received: 30 December 2022 Accepted: 29 June 2023
Published online: 10 July 2023

**References**

1. Rahmani, M., Vinasco, G., Rider, M. J., Romero, R., & Pardalos, P. M. (2013). Multistage transmission expansion planning considering fixed series compensation allocation. *IEEE Transactions on Power Systems, 28*(4), 3795–3805.
2. Xie, X., et al. (2017). Characteristic analysis of subsynchronous resonance in practical wind farms connected to series-compensated transmissions. *IEEE Transactions on Energy Conversion, 32*(3), 1117–1126.
3. Kumar, R., Diwania, S., Khetrapal, P., Singh, S., & Badoni, M. (2021). Multimachine stability enhancement with hybrid PSO-BFOA based PV-STATCOM. *Sustainable Computing Informatics and Systems*. https://doi.org/10.1016/j.suscom.2021.100615
4. Verma, N., Kumar, N., Gupta, S., Malik, H., Pedro, F., & Márquez, G. (2023). Review of sub: Synchronous interaction in wind integrated power systems—classification, challenges, and mitigation techniques. *Protection and Control of Modern Power Systems, 8*(1), 17.
5. Farmer, R. G., Schwalb, A. L., & Katz, E. (1977). Navajo project report on subsynchronous resonance analysis and solutions. *IEEE Transactions on Power Apparatus and Systems, 96*(4), 1226–1232.
6. Shair, J., Xie, X., Wang, L., Liu, W., He, J., & Liu, H. (2019). Overview of emerging subsynchronous oscillations in practical wind power systems. *Renewable and Sustainable Energy Reviews, 99*, 159–168.
7. Kundur, P., Klein, M., Rogers, G. J., & Zywno, M. S. (1989). Application of power system stabilizers for enhancement of overall system stability. *IEEE Power Engineering Review, 9*(5), 61.
8. Kumar, S., & Kumar, N. (2017). Alleviation SSR and low frequency power oscillations in series compensated transmission line using SVC supplementary controllers. *Journal of The Institution of Engineers (India): Series B, 98*(3), 255–266.
9. Piyasinghe, L., Miao, Z., Member, S., Khazaei, J., Fan, L., & Member, S. (2015). Impedance model-based SSR analysis for TCSC compensated type-3 wind energy delivery systems. *IEEE Transactions on Sustainable Energy, 6*(1), 179–187.
10. Mohammadpour, H. A., & Santi, E. (2015). Modeling and control of gate-controlled series capacitor interfaced with a DFIG-based wind farm. *IEEE Transactions on Industrial Electronics, 62*(2), 1022–1033.
11. Venkateswarlu, S., Janaki, M., & Thirumalaivasan, R. (2022). Analysis and mitigation of SSR in non-identical generators using multimodal BPF based SSDC. *ISA Transactions, 120*, 247–257.
12. Kumar, R., Diwania, S., Khetrapal, P., & Singh, S. (2022). Performance assessment of the two metaheuristic techniques and their hybrid for power system stability enhancement with PV-STATCOM. *Neural Computing and Applications, 34*(5), 3723–3744.
13. Jiang, H., et al. (2019). Application of UPFC to mitigate SSR in series-compensated wind farms. *J. Eng., 2019*(16), 2505–2509.
14. Liu, Y., Zheng, J., Chen, Q., Duan, Z., Tian, Y., Ban, M., & Li, Z. (2022). MMC-STATCOM supplementary wide-band damping control to mitigate subsynchronous control interaction in wind farms. *International Journal of Electrical Power & Energy Systems, 141*, 108171.
15. Kumar, R., Singh, R., & Ashfaq, H. (2020). Stability enhancement of induction generator–based series compensated wind power plants by alleviating subsynchronous torsional oscillations using BFOA-optimal controller tuned STATCOM. *Wind Energy, 23*(9), 1846–1867.
16. Kumar, R., Singh, R., & Ashfaq, H. (2020). Stability enhancement of multimachine power systems using ant colony optimization-based static synchronous compensator. *Computers & Electrical Engineering*. https://doi.org/10.1016/j.compeleceng.2020.106589
17. Yang, S., et al. (2022). PLL based sub-/super-synchronous resonance damping controller for D-PMSG wind farm integrated power systems. *IEEE Transactions on Energy Conversion, 37*(4), 2370–2384.
18. Ma, R., Han, Y., & Pan, W. (2021). Variable-gain super-twisting sliding mode damping control of series-compensated DFIG-based wind power system for SSCI mitigation. *Energies, 14*(2), 382.
19. Li, P., Xiong, L., Ma, M., Huang, S., Zhu, Z., & Wang, Z. (2022). Energy-shaping L2-gain controller for PMSG wind turbine to mitigate subsynchronous interaction. *International Journal of Electrical Power & Energy Systems, 135*, 107571.
20. Karunanayake, C., Ravishankar, J., & Dong, Z. Y. (2020). Nonlinear SSR damping controller for DFIG based wind generators interfaced to series compensated transmission systems. *IEEE Transactions on Power Systems, 35*(2), 1156–1165.
21. Kumar, R., Singh, R., Ashfaq, H., Singh, S. K., & Badoni, M. (2021). Power system stability enhancement by damping and control of sub-synchronous torsional oscillations using whale optimization algorithm based Type-2 wind turbines. *ISA Transactions, 108*, 240–256. https://doi.org/10.1016/j.isatra.2020.08.037
22. Gil-González, W., Montoya, O. D., & Garces, A. (2018). Control of a SMES for mitigating subsynchronous oscillations in power systems: A PBC-PI approach. *J. Energy Storage, 20*(June), 163–172.
23. Hemmati, R., Faraji, H., & Beigvand, N. Y. (2022). Multi objective control scheme on DFIG wind turbine integrated with energy storage system and FACTS devices: Steady-state and transient operation improvement. *International Journal of Electrical Power & Energy Systems, 135*, 107519.
24. Tsang, M. W., & Sutanto, D. (1998). Damping inter-area oscillation using a battery energy storage system. *Journal of Rheology (Melville, NY, United States), 450*, 409–414.
25. Zhu, Y., Liu, C., Sun, K., Shi, D., & Wang, Z. (2019). Optimization of battery energy storage to improve power system oscillation damping. *IEEE Transactions on Sustainable Energy, 10*(3), 1015–1024.
26. Khazaei, J., Asrari, A., Idowu, P., Shushekar, S., (2019). Sub-synchronous resonance damping using battery energy storage system. In *2018 North American Power Symposium*. NAPS 2018, pp 1–6.
27. Li, G., Chen, Y., Luo, A., & Wang, H. (2020). An enhancing grid stiffness control strategy of STATCOM/BESS for damping sub-synchronous resonance in wind farm connected to weak grid. *IEEE Transactions on Industrial Informatics, 16*(9), 5835–5845.
28. Ahmed, M. F., Mandor, M. A., El-Hadidy, M., & Bendary, F. M. (2021). Fuzzy based battery energy storage system and braking resistor for mitigation of shaft-torsional oscillations. *Journal of King Saud University-Engineering Sciences, 33*(8), 589–600.
29. Beza, M., & Bongiorno, M. (2015). An adaptive power oscillation damping controller by STATCOM with energy storage. *IEEE Transactions on Power Systems, 30*(1), 484–493.
30. Kumar, R., Diwania, S., Singh, R., Ashfaq, H., Khetrapal, P., & Singh, S. (2022). An intelligent Hybrid Wind–PV farm as a static compensator for overall stability and control of multimachine power system. *ISA Transactions, 123*, 286–302. https://doi.org/10.1016/j.isatra.2021.05.014
31. Verma, N., & Kumar, N. (2022). DFIG: Based wind plant coupled series compensated transmission line—modeling and SSR stability analysis. *Journal of The Institution of Engineers (India): Series B*. https://doi.org/10.1007/s40031-022-00807-6
32. Lei, Y., Mullane, A., Lightbody, G., & Yacamini, R. (2006). Modeling of the wind turbine with a doubly fed induction generator for grid integration studies. *IEEE Transactions on Energy Conversion, 21*(1), 257–264.
33. Fan, L., Kavasseri, R., Miao, Z. L., & Zhu, C. (2010). Modeling of DFIG-based wind farms for SSR analysis. *IEEE Transactions on Power Delivery, 25*(4), 2073–2082.
34. Mahalakshmi, R., & Sindhu Thampatty, K. C. (2020). Detailed modelling and development of a laboratory prototype for the analysis of subsynchronous resonance in DFIG-based wind farm. *International transactions on electrical energy systems, 30*(3), 1–22.
35. Eskandari, M., Rajabi, A., Savkin, A. V., Moradi, M. H., & Dong, Z. Y. (2022). Battery energy storage systems (BESSs) and the economy-dynamics of microgrids: Review, analysis, and classification for standardization of BESSs applications. *Journal of Energy Storage, 55*, 105627.
36. Chen, M., Member, S., & Rinc, G. A. (2006). Accurate electrical battery model capable of predicting runtime and I–V performance. *IEEE Transactions on Energy Conversion, 21*(2), 504–511.
37. Wu, T., Zhang, Y. J., & Tang, X. (2019). A VSC-based BESS Model for multi-objective OPF using mixed integer SOCP. *IEEE Transactions on Power Systems, 34*(4), 2541–2552.
38. Singh, S., Saini, S., Gupta, S. K., & Kumar, R. (2023). Solar-PV inverter for the overall stability of power systems with intelligent MPPT control of DC-link capacitor voltage. *Protection and Control of Modern Power, 8*, 15. https://doi.org/10.1186/s41601-023-00285-y

39. Singh, S. K., Singh, R., Ashfaq, H., & Kumar, R. (2022). Virtual Inertia emulation of inverter interfaced distributed generation (IIDG) for dynamic frequency stability & damping enhancement through BFOA Tuned optimal controller. *Arabian Journal for Science and Engineering., 47*, 3293–3310. https://doi.org/10.1007/s13369-021-06121-5
40. Padiar, K. R. (2012). *Analysis of subsynchronous resonance in power systems*. Springer Science & Business Media.
41. Khayyatzadeh, M., & Kazemzadeh, R. (2017). Sub-synchronous resonance damping using high penetration PV plant. *Mechanical Systems and Signal Processing, 84*, 431–444.
42. Shim, K. S., Kim, S. T., Lee, J. H., Choi, E. J., & Choi, J. H. (2014). Detection of low-frequency oscillation using synchrophasor in wide-area rolling blackouts. *International Journal of Electrical Power & Energy Systems, 63*, 1015–1022.
43. Rauhala, T., Gole, A. M., & Jarventausta, P. (2016). Detection of subsynchronous torsional oscillation frequencies using phasor measurement. *IEEE Transactions on Power Delivery, 31*(1), 11–19.
44. Joshi, P. M., & Verma, H. K. (2021). Synchrophasor measurement applications and optimal PMU placement: A review. *Electric Power Systems Research, 199*, 107428.